Adaptive Rectification Current Observer for slim DC-Link AC Drives with Unknown Input Voltage

Mohammad Ghousein, Thomas Devos, Nicolas Henwood, Al Kassem Jebai

Adaptive Rectification Current Observer for slim DC-Link AC Drives with Unknown Input Voltage

Mohammad Ghousein, Thomas Devos, Nicolas Henwood, Al Kassem Jebai

***Abstract*— The paper focuses on estimating the rectifier current in slim DC-Link AC drives, known for their reduced DC-Link capacitance. Particularly, at full load, the capacitor's filtering effect on the input voltage diminishes. This allows the estimation of the input voltage from DC-Link voltage measurements. We adopt a simplified model, treating the drive as a DC-Link that supplies a constant power load. Notably, the model accounts for the equivalent series resistance (ESR) of the capacitor, adding intricacy to the design. We propose an adaptive observer to estimate both the rectification current and the input voltage. We design a Luenberger state observer with output injection terms. The study on the observer stability is based on decoupling the state estimation errors from the input estimation errors through swapping design. Theoretical developments are validated through numerical simulations.**

I. Introduction

Three phase electrical motor drives equipped with voltage source PWM inverters are used in many applications such as Heating, Ventilation, Air-Conditioning (HVAC) [1], electric vehicles [2], water and wastewater treatment [3], oil and gas industry [4], etc. A typical motor drive system employing a front-end diode rectifier is shown in Figure 1. The 6-pulse diode bridge rectifies the three-phase voltages $(V_A(t), V_B(t), V_C(t))$. The role of the capacitor at the output of the rectifier is to filter the rectified voltage. The resulting DC-link voltage across the capacitor is then modulated by the inverter to generate three-phase voltage signals, enabling precise control of the motor's speed or torque. For applications with low dynamic performance requirements such as the HVAC applications [5], the DC-Link capacitance can be reduced. In the literature, AC drives with small DC-Link capacitance are called slim DC-Link AC drives [6]. Such types of drives have low cost and low total harmonic distortion (THD) of the grid current. In addition, the DC-Link electrolytic capacitors can be replaced by film capacitors [7].

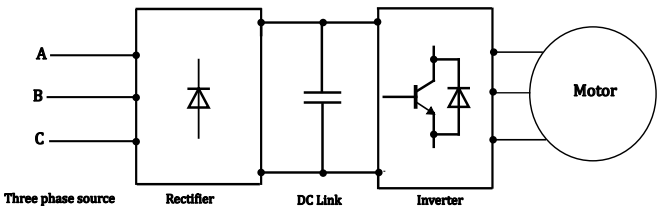

Fig. 1. Three phase drive system.

The authors are with the motor control department at Schneider Electric. E-mails: {mohammad.ghousein}@non.se.com {thomas.devos,nicolas.henwood, al-kassem.jebai}@se.com

The three phase circuit of Figure 1 can be simplified to have the single phase circuit shown in Figure 2 (see [8], [9], [10] and references therein). We recall here the definition of the

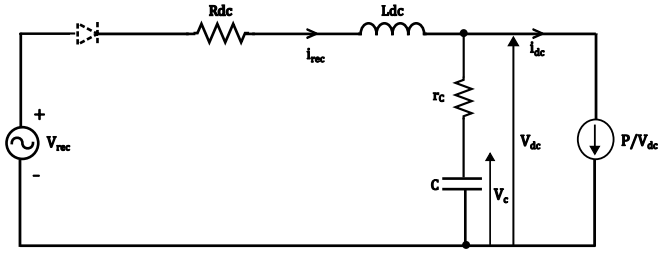

Fig. 2. Simplified drive circuit.

circuit variables

$$\begin{aligned} R_{dc} &= 2R_{cc} + 2r_d + 6F_{cc}L_{cc} \\ L_{dc} &= 2L_{cc} \end{aligned} \tag{1}$$

where F_{cc} is the grid frequency, R_{cc} is the source resistance, L_{cc} is the source inductance, r_d is the diode bridge on-resistance, C is the DC-Link capacitance, r_C is the ESR, P is the power consumed by the motor, $i_{rec}(t)$ is the rectification current and $V_{dc}(t)$ is the DC-Link voltage. The resistance $6F_{cc}L_{cc}$ in (1) models the commutation effect of the 6-pulse diode bridge. The three phase inverter and the motor are modeled as a constant power load of current $i_{dc}(t)$ inversely proportional to the DC-Link voltage $V_{dc}(t)$. For an electrical grid with nominal line-line RMS voltage U_N, the rectification voltage can be expressed as [9]:

$$V_{rec}(t) = V_{avg} + 2V_{avg}\sum_{n=1}^{+\infty}\frac{(-1)^n}{1-36n^2}cos(12\pi F_{cc}nt) \tag{2}$$

with $V_{avg} = 3\sqrt{2}U_N/\pi$. Since the capacitance C is small, the capacitor filtering effect is almost neglected at full load. The DC-Link voltage $V_{dc}(t)$ and the input voltage $V_{rec}(t)$ have similar dynamics. The idea is to estimate $V_{rec}(t)$ and $i_{rec}(t)$ simultaneously from the DC-Link voltage measurements. More precisely, we consider that

$$V_{rec}(t) \approx F^\top(t)\theta \tag{3}$$

with

$$F(t) = \begin{pmatrix} 1 \\ cos\big(12\pi(Fcc)t\big) \\ cos\big(12\pi(2Fcc)t\big) \\ \vdots \\ cos\big(12\pi(mFcc)t\big) \end{pmatrix}, \theta = \begin{pmatrix} \theta_0 \\ \theta_1 \\ \vdots \\ \theta_m \end{pmatrix} \tag{4}$$

where θ_0 is V_{avg} and $\theta_1, \ldots, \theta_m$ are the amplitudes of the first, $\ldots$, m^{th} harmonic respectively. The harmonics amplitudes θ are considered to be unknown while the harmonics spectrum $F(t)$ is considered to be known. The aim of this paper is to simultaneously estimate θ and $i_{rec}(t)$ using $V_{dc}(t)$. Notably, input voltage measurements are not always available in drive systems. In the estimation problem considered in this paper, the input voltage measurements are not required. Only grid frequency information is needed.

Observers for the rectification current $i_{rec}(t)$ are not widely studied in the literature. In [11], the authors proposed a Luenberger observer for the rectification current aiming for active DC-Link stabilization. The observer considers that the source $V_{rec}(t)$ is constant and unknown. The ESR was neglected, and only the DC component of $V_{rec}(t)$ was estimated. In [12], the authors introduced a sliding mode observer for the unknown power P and the rectification current $i_{rec}(t)$ in DC-Link stabilization. For constant power loads in DC micro grids, the authors [13] proposed a nonlinear disturbance observer to estimate the input voltage variations and the parameters variations. Inspired by [11], we propose an adaptive observer to estimate the amplitudes of the rectification voltage harmonics as well as the rectification current for slim DC-Link AC drives. Our DC-Link model accounts for the ESR resistance, and we employ the swapping design method [14] to decouple the state estimation errors from the inputs estimation errors. The convergence of the observer is proved via Lyapunov analysis. In practical terms, the input $V_{rec}(t)$ is an ideal voltage source that cannot be directly measured. The adaptation scheme outlined in this paper for $V_{rec}(t)$ assists in accurately estimating the rectifier current $i_{rec}(t)$. This estimation is crucial for stabilizing the DC-Link voltage in slim DC-Link AC Drives.

The paper is organized as follows: in Section II we present the model of the DC-Link under constant power load, incorporating the ESR resistance. The adaptive observer architecture is detailed in Section III. Section IV is dedicated to the stability analysis of the adaptive observer. Section V presents the simulation results, while concluding remarks are provided in Section VI.

Notation

The symbols S_+^n represent the set of real $n \times n$ symmetric positive definite matrices. For a symmetric matrix A, positive and negative definiteness are denoted, respectively, by $A \succ 0$ and $A \prec 0$. For a vector $z \in \mathbb{R}^n$, $\left|z\right|_1 = \sum_{i=1}^n |z_i|$ and $\left|z\right|_2 = \sqrt{\sum_{i=1}^n z_i^2}$. The space of all signals that are globally bounded is denoted by $\mathcal{L}_\infty$.

II. Model Presentation

Consider the single phase circuit of Figure 2. Using basic circuit analysis, the system dynamics are

$$L_{dc}\frac{di_{rec}(t)}{dt} = V_{rec}(t) - R_{dc}i_{rec}(t) - V_{dc}(t) \tag{5}$$

$$C\frac{dV_c(t)}{dt} = i_{rec}(t) - \frac{P}{V_{dc}(t)} \tag{6}$$

$$V_{dc}(t) = r_C C\frac{dV_c(t)}{dt} + V_c(t) \tag{7}$$

where $i_{rec}(t)$ is the rectification current and $V_c(t)$ is the capacitor voltage. We assume that P is sufficiently large so that the rectification current $i_{rec}(t)$ is always positive. The virtual diode shown in Figure 2 has no effect in this case. Now, we consider that $i_{rec}(t)$ and $V_{dc}(t)$ are the system states. The dynamics of the rectification current $i_{rec}(t)$ is already defined as a function of $V_{dc}(t)$. Our goal is to calculate the dynamics of the DC-Link voltage $V_{dc}(t)$. Differentiate (7) in time and substitute (6) and (5) to get

$$\begin{aligned}\frac{dV_{dc}(t)}{dt} = &\left(\frac{1}{C} - \frac{r_C R_{dc}}{L_{dc}}\right)\frac{V_{dc}^2(t)}{V_{dc}^2(t) - r_C P}i_{rect}(t) \\ &- \frac{r_C}{L_{dc}}\frac{V_{dc}^3(t)}{V_{dc}^2(t) - r_C P} - \frac{V_{dc}(t)}{V_{dc}^2(t) - r_C P}\frac{P}{C} \\ &+ \frac{V_{dc}^2(t)}{V_{dc}^2(t) - r_C P}\frac{r_C}{L_{dc}}V_{rec}(t)\end{aligned} \tag{8}$$

Equation (5) and equation (8) model the dynamics of the circuit shown in Figure 2 with $r_C \neq 0$. The inputs of the system are the rectification voltage $V_{rec}(t)$ and the power P. The output of the system is the DC-Link voltage $V_{dc}(t)$. The input $V_{rec}(t)$ is approximated by the harmonic decomposition in (4). The DC-Link model becomes

$$\frac{di_{rec}(t)}{dt} \approx \frac{1}{L_{dc}}F^\top(t)\theta - \frac{R_{dc}}{L_{dc}}i_{rec}(t) - \frac{1}{L_{dc}}V_{dc}(t) \tag{9}$$

$$\begin{aligned}\frac{dV_{dc}(t)}{dt} \approx &\left(\frac{1}{C} - \frac{r_C R_{dc}}{L_{dc}}\right)\frac{V_{dc}^2(t)}{V_{dc}^2(t) - r_C P}i_{rect}(t) \\ &- \frac{r_C}{L_{dc}}\frac{V_{dc}^3(t)}{V_{dc}^2(t) - r_C P} - \frac{V_{dc}(t)}{V_{dc}^2(t) - r_C P}\frac{P}{C} \\ &+ \frac{V_{dc}^2(t)}{V_{dc}^2(t) - r_C P}\frac{r_C}{L_{dc}}F^\top(t)\theta\end{aligned} \tag{10}$$

Our goal is to estimate $i_{rec}(t)$ and θ given the measurements of the DC-Link voltage $y(t) = V_{dc}(t)$ and the power P.

III. Adaptive Observer Design

We denote by $\hat{i}_{rec}(t)$ the estimated value of $i_{rec}(t)$, $\hat{V}_{dc}(t)$ the estimated value of $V_{dc}(t)$ and $\hat{\theta}(t)$ the estimated value

of θ. We introduce the following adaptive observer design

$$\begin{aligned}\frac{d\hat{i}_{rec}(t)}{dt} &= \frac{1}{L_{dc}}F^{\top}(t)\hat{\theta}(t) - \frac{R_{dc}}{L_{dc}}\hat{i}_{rec}(t) - \frac{1}{L_{dc}}\hat{V}_{dc}(t) \\ &+ L_1(y(t) - \hat{V}_{dc}(t)) + m_1(t)\end{aligned} \tag{11}$$

$$\begin{aligned}\frac{d\hat{V}_{dc}(t)}{dt} &= (\frac{1}{C} - \frac{r_C R_{dc}}{L_{dc}})\frac{y^2(t)}{y^2(t) - r_C P}\hat{i}_{rect}(t) \\ &- \frac{r_C}{L_{dc}}\frac{y^3(t)}{y^2(t) - r_C P} - \frac{y(t)}{y^2(t) - r_C P}\frac{P}{C} \\ &+ \frac{y^2(t)}{y^2(t) - r_C P}\frac{r_C}{L_{dc}}F^{\top}(t)\hat{\theta}(t) \\ &+ L_2(y(t) - \hat{V}_{dc}(t)) + m_2(t)\end{aligned} \tag{12}$$

where L_1 and L_2 are two observer gains to be designed later. The signals $m_1(t)$ and $m_2(t)$ are two feedback gains to be defined later. Now, we define the estimation error variables: $\tilde{i}_{rec}(t) = i_{rec}(t) - \hat{i}_{rec}(t)$, $\tilde{V}_{dc}(t) = V_{dc}(t) - \hat{V}_{dc}(t)$ and $\tilde{\theta}(t) = \theta - \hat{\theta}(t)$. By subtracting (11)-(12) from (9)-(10), we obtain the following error dynamics

$$\begin{aligned}\frac{d\tilde{i}_{rec}(t)}{dt} &= \frac{1}{L_{dc}}F^{\top}(t)\tilde{\theta}(t) - \frac{R_{dc}}{L_{dc}}\tilde{i}_{rec}(t) - L_1^{'}\tilde{V}_{dc}(t) \\ &- m_1(t)\end{aligned} \tag{13}$$

$$\begin{aligned}\frac{d\tilde{V}_{dc}(t)}{dt} &= (\frac{1}{C} - \frac{r_C R_{dc}}{L_{dc}})\frac{y^2(t)}{y^2(t) - r_C P}\tilde{i}_{rect}(t) - L_2\tilde{V}_{dc}(t) \\ &+ \frac{y^2(t)}{y^2(t) - r_C P}\frac{r_C}{L_{dc}}F^{\top}(t)\tilde{\theta}(t) - m_2(t)\end{aligned} \tag{14}$$

where $L_1^{'} = \frac{1}{L_{dc}} + L_1$. The observer in (11)-(12) is of Luenberger type, which is a copy of the original system with output injections $y(t)$, and two additional feedback gains $m_1(t)$ and $m_2(t)$. Our goal is to find L_1, L_2, $m_1(t)$, $m_2(t)$ and a proper adaptive law for θ so that the error system (13)-(14) converge to zero.

IV. Observer Stability Analysis

The first step is to decouple the state estimation errors $\tilde{i}_{rec}(t)$, $\tilde{V}_{dc}(t)$ from the input estimation errors $\tilde{\theta}(t)$ using the swapping design method. The idea of the swapping method is to parameterize the state estimation errors $\tilde{i}_{rec}(t)$, $\tilde{V}_{dc}(t)$ using K-filters (see [14]) as follows

$$\tilde{i}_{rec}(t) = \tilde{i}^n_{rec}(t) - R^{\top}(t)\tilde{\theta}(t) \tag{15}$$

$$\tilde{V}_{dc}(t) = \tilde{V}^n_{dc}(t) - N^{\top}(t)\tilde{\theta}(t) \tag{16}$$

where $R(t)$ and $N(t)$ are K-filters given by

$$R(t) = \begin{pmatrix} R_0(t) \\ R_1(t) \\ \vdots \\ R_m(t) \end{pmatrix}, N(t) = \begin{pmatrix} N_0(t) \\ N_1(t) \\ \vdots \\ N_m(t) \end{pmatrix} \tag{17}$$

$\tilde{i}^n_{rec}(t)$ and $\tilde{V}^n_{dc}(t)$ are the states estimation errors if the input is known i.e. $\tilde{\theta}(t) = 0$. Differentiate (15) in time and substitute (13) and (16) to get

$$\begin{aligned}\frac{d\tilde{i}^n_{rec}(t)}{dt} &= -\frac{R_{dc}}{L_{dc}}\tilde{i}^n_{rec}(t) - L_1^{'}\tilde{V}^n_{dc}(t) + R^{\top}(t)\frac{d\tilde{\theta}}{dt}(t) - m_1(t) \\ &+ \Big(\frac{dR^{\top}}{dt}(t) + \frac{R_{dc}}{L_{dc}}R^{\top}(t) + L_1^{'}N^{\top}(t) \\ &+ \frac{1}{L_{dc}}F^{\top}(t)\Big)\tilde{\theta}(t)\end{aligned} \tag{18}$$

In the same way, differentiate (16) in time and substitute (14) and (15) to have

$$\begin{aligned}\frac{d\tilde{V}^n_{dc}(t)}{dt} &= (\frac{1}{C} - \frac{r_C R_{dc}}{L_{dc}})\frac{y^2(t)}{y^2(t) - r_C P}\tilde{i}^n_{rec}(t) - L_2\tilde{V}^n_{dc}(t) \\ &+ N^{\top}(t)\frac{d\tilde{\theta}}{dt}(t) - m_2(t) + \Big(\frac{dN^{\top}}{dt}(t) + L_2N^{\top}(t) \\ &- (\frac{1}{C} - \frac{r_C R_{dc}}{L_{dc}})\frac{y^2(t)}{y^2(t) - r_C P}R^{\top}(t) \\ &+ \frac{y^2(t)}{y^2(t) - r_C P}\frac{r_C}{L_{dc}}F^{\top}(t)\Big)\tilde{\theta}(t)\end{aligned} \tag{19}$$

Equations (18)-(19) suggest the following dynamics

1) **Observation error dynamics**

$$\begin{aligned}\frac{d\tilde{i}^n_{rec}(t)}{dt} &= -\frac{R_{dc}}{L_{dc}}\tilde{i}^n_{rec}(t) - L_1^{'}\tilde{V}^n_{dc}(t) \\ \frac{d\tilde{V}^n_{dc}(t)}{dt} &= (\frac{1}{C} - \frac{r_C R_{dc}}{L_{dc}})v(t)\tilde{i}^n_{rect}(t) - L_2\tilde{V}^n_{dc}(t)\end{aligned} \tag{20}$$

2) **K-filter dynamics**

$$\begin{aligned}\frac{dR(t)}{dt} &= -\frac{R_{dc}}{L_{dc}}R(t) - L_1^{'}N(t) - \frac{1}{L_{dc}}F(t) \\ \frac{dN(t)}{dt} &= (\frac{1}{C} - \frac{r_C R_{dc}}{L_{dc}})v(t)R(t) - L_2N(t) \\ &- v(t)\frac{r_C}{L_{dc}}F(t)\end{aligned} \tag{21}$$

3) **Feedback Gains**

$$\begin{aligned}m_1(t) &= R^{\top}(t)\frac{d\tilde{\theta}(t)}{dt} = -R^{\top}(t)\frac{d\hat{\theta}(t)}{dt} \\ m_2(t) &= N^{\top}(t)\frac{d\tilde{\theta}(t)}{dt} = -N^{\top}(t)\frac{d\hat{\theta}(t)}{dt}\end{aligned} \tag{22}$$

4) **Output dependent term**

$$v(t) = \frac{y^2(t)}{y^2(t) - r_C P} \tag{23}$$

Equation (16) also suggests the following normalized adaptation law:

$$\frac{d\hat{\theta}(t)}{dt} = -\frac{d\tilde{\theta}(t)}{dt} = -\frac{P_\theta(t)N(t)}{1 + N^{\top}(t)N(t)}\tilde{V}_{dc}(t) \tag{24}$$

$$\frac{dP_\theta(t)}{dt} = \beta P_\theta(t) - \frac{P_\theta(t)N(t)N^{\top}(t)P_\theta(t)}{1 + N^{\top}(t)N(t)} \tag{25}$$

$P_\theta(t) \in S_+^{m+1}$ and $\beta > 0$ is the forgetting factor. The initial conditions $\hat{\theta}(0) = \hat{\theta}_0$ and $P_\theta(0)$=$P_{\theta,0}$=$P_{\theta,0}^T$ are chosen arbitrary. It is useful to illustrate that the adaptation law (24)-(25) is derived using the superposition principle, i.e. fix $\tilde{V}_{dc}^n(t)$ to zero in order to get the linear regressor equation

$$\tilde{V}_{dc}(t) = -N^T(t)\tilde{\theta}(t) \tag{26}$$

Then using (26), choose the adaptation law (24)-(25) to estimate θ. The adaptive law (24)-(25) is called continuous time recursive least square estimator with a forgetting factor (see [15] for various linear regression estimation techniques). Using (24) and (16), compute the dynamics of the input estimation errors $\tilde{\theta}(t)$ as follows

$$\frac{d\tilde{\theta}(t)}{dt} = \frac{P_\theta(t)N(t)}{1 + N^T(t)N(t)}\big(\tilde{V}_{dc}^n(t) - N^\top(t)\tilde{\theta}(t)\big) \tag{27}$$

In view of equations (15)-(16) and the derived dynamics (20), the states estimation errors $(\tilde{i}_{rec}(t), \tilde{V}_{dc}(t))$ splits into two parts: 1) an observation error $(\tilde{i}_{rec}^n(t), \tilde{V}_{dc}^n(t))$ that is totally decoupled from $\tilde{\theta}(t)$, and 2) an induced error due to the parameters mismatch $N(t)\tilde{\theta}(t)$ and $R(t)\tilde{\theta}(t)$ which is proportional to the input parameter estimation errors $\tilde{\theta}(t)$. To prove the convergence of $(\tilde{i}_{rec}(t), \tilde{V}_{dc}(t), \tilde{\theta}(t))$ it is sufficient to prove the convergence of $(\tilde{i}_{rec}^n(t), \tilde{V}_{dc}^n(t), \tilde{\theta}(t))$ and the boundedness of the filters $R(t)$ and $N(t)$. This is what we establish in the following series of Lemmas.

Remark 1: The output dependent term $v(t)$ is equal to 1 if $r_C = 0$. Actually, for an electric drive which is correctly sized and operating at the nominal power P, we have that

$$y^2(t) >> r_C P \tag{28}$$

which means

$$v(t) = \frac{y^2(t)}{y^2(t) - r_C P} \approx 1 \tag{29}$$

From now on, we replace $v(t)$ by 1 in view of the plant assumption (29).

Lemma 1: Consider the observation error dynamics (18)-(20) with initial conditions $(\tilde{i}_{rec}^n(0), \tilde{V}_{dc}^n(0))$. If

$$L_1 = \frac{1}{\big(\frac{1}{C} - \frac{r_C R_{dc}}{L_{dc}}\big)}\big(\lambda_1 - \frac{R_{dc}}{L_{dc}}\big)\big(\lambda_2 - \frac{R_{dc}}{L_{dc}}\big) - \frac{1}{L_{dc}} \tag{30}$$

$$L_2 = -\frac{R_{dc}}{L_{dc}} + \lambda_1 + \lambda_2 \tag{31}$$

for any $\lambda_1 > 0$ and $\lambda_2 > 0$. Then, the observation error dynamics $(\tilde{i}_{rec}^n(t), \tilde{V}_{dc}^n(t))$ is exponentially stable.

Proof 1: Let $\tilde{x}(t) = (\tilde{i}_{rec}^n(t), \tilde{V}_{dc}^n(t))^\top$. The observation error dynamics can be written as

$$\frac{d\tilde{x}(t)}{dt} = A_d\tilde{x}(t) \tag{32}$$

with $A_d = A - LC$ such as

$$A = \begin{pmatrix} -\frac{R_{dc}}{L_{dc}} & -\frac{1}{L_{dc}} \\ \big(\frac{1}{C} - \frac{r_C R_{dc}}{L_{dc}}\big) & 0 \end{pmatrix}, L = \begin{pmatrix} L_1 \\ L_2 \end{pmatrix}, C = \begin{pmatrix} 0 & 1 \end{pmatrix} \tag{33}$$

By inserting (30)-(31) in A_d, one can find that $-\lambda_1$ and $-\lambda_2$ are the eigenvalues of A_d. Since the couple (A, C) is observable, $-\lambda_1$ and $-\lambda_2$ can be chosen anywhere in the left half of the complex plane. Since the eigenvalues of A_d are less than zero, then there exists $P \in S_+^2$ such that

$$A_d^\top P + PA_d = -Q \tag{34}$$

The Lyapunov equation (34) has a unique solution P for every predefined $Q \in S_+^2$. Furthermore, it is easy to verify that

$$\tilde{\tilde{i}}_{rec}(t) = A_1 e^{-\lambda_1 t} + A_2 e^{-\lambda_2 t} \tag{35}$$

$$\tilde{V}_{dc}(t) = B_1 e^{-\lambda_1 t} + B_2 e^{-\lambda_2 t} \tag{36}$$

is the solution of (32) for $\lambda_1 \neq \lambda_2$, where A_1, A_2, B_1, B_2 are constants depending on the initial conditions $(\tilde{i}_{rec}^n(0), \tilde{V}_{dc}^n(0))$. From (35)-(36), we deduce that the solution converge to zero, $\tilde{\tilde{i}}_{rec}(t) \in \mathcal{L}_\infty$ and $\tilde{V}_{dc}(t) \in \mathcal{L}_\infty$. The proof is complete.

Lemma 2: Consider the K-filters $R(t) \in \mathbb{R}^{m+1}$ and $N(t) \in \mathbb{R}^{m+1}$ with zero initial conditions $R(0) = 0$ and $N(0) = 0$. If L_1 and L_2 are chosen as in (30)-(31), then $R(t) \in \mathcal{L}_\infty$, $N(t) \in \mathcal{L}_\infty$.

Proof 2: The K-filters in (21) can be written as

$$\dot{K}_i(t) = A_d K_i(t) + BF_i(t) \tag{37}$$

where $K_i(t) = (R_i(t), N_i(t))^\top$ for every $0 \leq i \leq m$. B is the constant matrix given by $B = -\frac{1}{L_{dc}}(1, r_C)^\top$. From the definition of $F(t)$ given in (4), we have

$$F_i(t) \leq 1 \quad \forall \quad 0 \leq i \leq m \tag{38}$$

The system (37) is a linear time invariant system with bounded input $F_i(t)$. Since A_d is exponentially stable (by the choice of L_1 and L_2 in (30)-(31)), then $K_i(t)$ is bounded for every $0 \leq i \leq m$. By this, the proof ends.

Lemma 3: If $N(t)$ is bounded and persistently exciting (PE), i.e. for all $t \geq 0$ there exist positive constants T_0, c_0 and c_1 such that

$$c_0 I \leq \int_t^{t+T_0} N(\tau)N^\top(\tau)d\tau \leq c_1 I \tag{39}$$

where $I \in \mathbb{R}^{m+1}$ is the identity matrix. Then, there exists four positive constants α_0,α_1,β_0,β_1 such that

$$\begin{aligned} \alpha_0 I \leq P_\theta(t) \leq \alpha_1 I \\ \beta_0 I \leq P_\theta^{-1}(t) \leq \beta_1 I \end{aligned} \tag{40}$$

The matrix $P_\theta^{-1}(t) \in S_+^{m+1}$ (the inverse of $P_\theta(t)$) can be calculated by

$$\frac{dP_\theta^{-1}(t)}{dt} = -\beta P_\theta^{-1}(t) + \frac{N(t)N^\top(t)}{1 + N^T(t)N(t)} \tag{41}$$

Proof 3: See corollary 4.3.2 in [15].

Now, consider the Lyapunov function for the input estimation errors

$$V(t) = \frac{1}{2}\tilde{\theta}^\top(t)P_\theta^{-1}(t)\tilde{\theta}(t) \tag{42}$$

Differentiate (42) in time and substitute (27) to have

$$\begin{aligned}\frac{dV(t)}{dt} &= \frac{N^\top(t)\tilde{\theta}(t)}{1+N^\top(t)N(t)}\tilde{V}_{dc}^n(t) \\ &\quad - \frac{1}{2}\tilde{\theta}^\top(t)\left(\beta P_\theta^{-1}(t) + \frac{N(t)N^\top(t)}{1+N^T(t)N(t)}\right)\tilde{\theta}(t)\end{aligned} \tag{43}$$

The last term of (43) is always negative if $N(t)$ is persistently exciting by Lemma 3. Let us look on the first term of (43)

$$\begin{aligned}\frac{N^\top(t)\tilde{\theta}(t)}{1+N^\top(t)N(t)}\tilde{V}_{dc}^n(t) &\leq |N^\top(t)\tilde{\theta}(t)||\tilde{V}_{dc}^n(t)| \\ &\leq N_{max}\big|\tilde{\theta}(t)\big|_1|\tilde{V}_{dc}^n(t)| \\ &\leq N_{max}\sqrt{m+1}\big|\tilde{\theta}(t)\big|_2|\tilde{V}_{dc}^n(t)| \\ &\leq G|\tilde{V}_{dc}^n(t)|\sqrt{V(t)}\end{aligned} \tag{44}$$

where N_{max} is the bound on $N(t)$ given in Lemma 2 and G is a positive constant given by

$$G = \sqrt{\frac{2(m+1)}{\beta_0}}N_{max} \tag{45}$$

To prove (44), we have used: the triangle inequality $|x+y| \leq |x|+|y|$, the equivalency of norms in $\mathbb{R}^n$ i.e. $\big|x\big|_1 \leq \sqrt{n}\big|x\big|_2$ and the fact that

$$\frac{1}{2}\beta_0\big|\tilde{\theta}\big|_2^2 \leq V(t) \leq \frac{1}{2}\beta_1\big|\tilde{\theta}\big|_2^2 \tag{46}$$

Now using (43) and (44), one can obtain the following bound on the derivative of the Lyapunov function

$$\frac{dV(t)}{dt} \leq G|\tilde{V}_{dc}^n(t)|\sqrt{V(t)} \tag{47}$$

By integrating (47) in the interval $[0,t]$, we calculate the following bound on the Lyapunov function

$$\sqrt{V(t)} \leq \sqrt{V(0)} + \frac{G}{2}\int_0^t |\tilde{V}_{dc}^n(\tau)|d\tau \tag{48}$$

Therefore, the estimation error is bounded by above as

$$\big|\tilde{\theta}(t)\big|_2 \leq \big|\tilde{\theta}(0)\big|_2 + \frac{G}{2\sqrt{\beta_0}}\int_0^t |\tilde{V}_{dc}^n(\tau)|d\tau \tag{49}$$

Hence, $\tilde{\theta}(t) \in \mathcal{L}_\infty$ and $V(t) \in \mathcal{L}_\infty$. By (47), the boundedness of $V(t)$ and the convergence of $\tilde{V}_{dc}^n(t)$ to zero, we have $\lim_{t\to\infty}\frac{dV(t)}{dt} = 0$ (see similar proof in [16, equation (11)]). By (43), since $P_\theta^{-1}(t)$ and $N(t)N^\top(t)$ are positive definite, this means that $\lim_{t\to\infty}\tilde{\theta}(t) = 0$. From (15)-(16) and the boundedness of the K-filters in Lemma 2, then $\lim_{t\to\infty}\tilde{i}_{rec}(t) = 0$ and $\lim_{t\to\infty}\tilde{V}_{dc}(t) = 0$.

V. Numerical Simulations

The parameters used in the simulations are

- Electrical grid parameters: $U_N = 400\,\text{V}$ and $F_{cc} = 50\,\text{Hz}$. The grid resistance and the grid inductance corresponds to a $10\,\text{kA}$ electrical grid and they are $R_{cc} = 7\,\text{m}\Omega$ and $L_{cc} = 70\,\mu\text{H}$.

Harmonics	Amplitude
0 Hz	540.2 V
300 Hz	30.87 V
600 Hz	−7.55 V
900 Hz	3.34 V
1.2 KHz	−1.87 V
1.5 KHz	1.2 V
1.8 KHz	−0.83 V
2.1 KHz	0.61 V
2.4 KHz	−0.46 V

TABLE I

Amplitudes of the first eight harmonics of $V_{rec}(t)$

- Electrical drive parameters ($11\,\text{kW}$): the diode bridge on-resistance is $r_d = 5\,\text{m}\Omega$, the capacitance $C = 12\,\mu\text{F}$ and the ESR $r_C = 0.575\,\Omega$.

From (1), one can calculate the equivalent circuit parameters to have: $R_{dc} = 45\,\text{m}\Omega$ and $L_{dc} = 140\,\mu\text{H}$. The simulations are conducted in two steps: the first step is to simulate the model (5)-(7) to get the DC-Link voltage measurement $y(t) = V_{dc}(t)$. The second step is to inject $y(t)$ in the adaptive observer (11), (12) and (24) to estimate the rectification current $i_{rec}(t)$ and the harmonics of the rectification input $V_{rec}(t)$.

A. Step 1: Model Simulation

The model (5)-(8) is simulated in Matlab2022a with a fixed step solver (ode3). The time step is $T_s = 10\,\mu\text{s}$. The initial conditions are: $i_{rec}(0) = 0\,\text{A}$ and $V_{dc}(0) = 540\,\text{V}$. The load power is fixed to $P = 7.5\,\text{kW}$ and the rectification voltage $V_{rec}(t)$ is calculated as

$$\begin{aligned}V_{rec}(t) = \max\big\{&|V_A(t) - V_B(t)|, |V_B(t) - V_C(t)|, \\ &|V_C(t) - V_A(t)|\big\}\end{aligned} \tag{50}$$

where $V_A(t)$, $V_B(t)$ and $V_C(t)$ are three ideal grid sources given by

$$\begin{aligned}V_A(t) &= U_N\sqrt{(2/3)}sin(2\pi F_{cc}t) \\ V_B(t) &= U_N\sqrt{(2/3)}sin(2\pi F_{cc}t - 2\pi/3) \\ V_C(t) &= U_N\sqrt{(2/3)}sin(2\pi F_{cc}t + 2\pi/3)\end{aligned} \tag{51}$$

Note that $V_{rec}(t)$ in (2) is the Fourier series decomposition of (50). The output DC-Link voltage $y(t) = V_{dc}(t)$ of the model is injected in the adaptive observer.

B. Step 2: Adaptive Observer Simulation

To simulate the adaptive observer (11)-(12), one must know the following parameters (in addition to the circuit parameters): the load power P, the number of harmonics m, the observer gains L_1 and L_2 and the forgetting factor β. The power P is same as the model $P = 7.5\,\text{kW}$. The number of harmonics is $m = 8$. In Table I, we list the amplitudes of the first eight harmonics of $V_{rec}(t)$ (see (2)). The number of harmonics that can be estimated by the observer depends on the dynamics of the measurement $y(t) = V_{dc}(t)$. It is impossible to estimate an input harmonic if it is not present in the measurement. In the case of slim DC-Link AC drives, the capacitor plays a minor role in filtering the input voltage

especially if P is not very small (light load). In this case, the input harmonics with significant amplitudes are present in the DC-Link voltage $y(t)$. The observer gains L_1 and L_2 are calculated by (30)-(31). The eigenvalues of A_d are placed at $\lambda_1 = -1$ and $\lambda_2 = -5$ which leads to $L_1 = -7141.6$ and $L_2 = -315.4$. The forgetting factor is set to $\beta = 0.1$. The adaptive observer is started from the following initial conditions: $\hat{i}_{rec}(0) = 0$, $\hat{V}_{dc}(0) = 490\,\mathrm{V}$ and $\hat{\theta}(0) = 0$. The right column of Figure 3 shows that the observer succeeds in estimating the rectification current $i_{rec}(t)$ with an error less than $1\,\mathrm{A}$. The rectification voltage $V_{rec}(t)$ and the DC-Link voltage $V_{dc}(t)$ are estimated with absolute errors less than $10\,\mathrm{V}$. The left column shows the estimated current and the estimated voltages at $t = 7$ seconds. The observer captures the transients of the system although the input $V_{rec}(t)$ is not completely known. The swapping error systems $\tilde{x}(t)$ and $\tilde{\theta}(t)$ are shown in Figure 4. The observation error system $\tilde{x}(t)$ converges after 5 seconds. The convergence time is completely controllable by the position of the poles of A_d. It is interesting to notice that the error on the estimation amplitudes $\left|\tilde{\theta}(t)\right|$ increases with the harmonics frequency. As the frequency increases, the capacitor starts to filter the input amplitudes. This results in removing the signature of the high frequencies from the measurement $V_{dc}(t)$. Figure 4 shows an error of less than $0.1\,\mathrm{V}$ on all the estimated harmonics. This shows that the adaptive observer is capable of estimating the first eight harmonics of the input. Recall that this capability is inherited from the fact that the capacitor is small in such slim AC Drives. Finally, the Lyapunov function $V(t)$ is shown in Figure 5. Between 0 and 2 seconds, $V(t)$ is not always decreasing. Indeed, the dynamics of $V(t)$ are not linked only to $\tilde{\theta}(t)$ but also to $\tilde{x}(t)$ (see (43)). Figure 4 shows that when $\tilde{x}(t)$ starts to decrease, the Lyapunov function $V(t)$ starts to decrease as well.

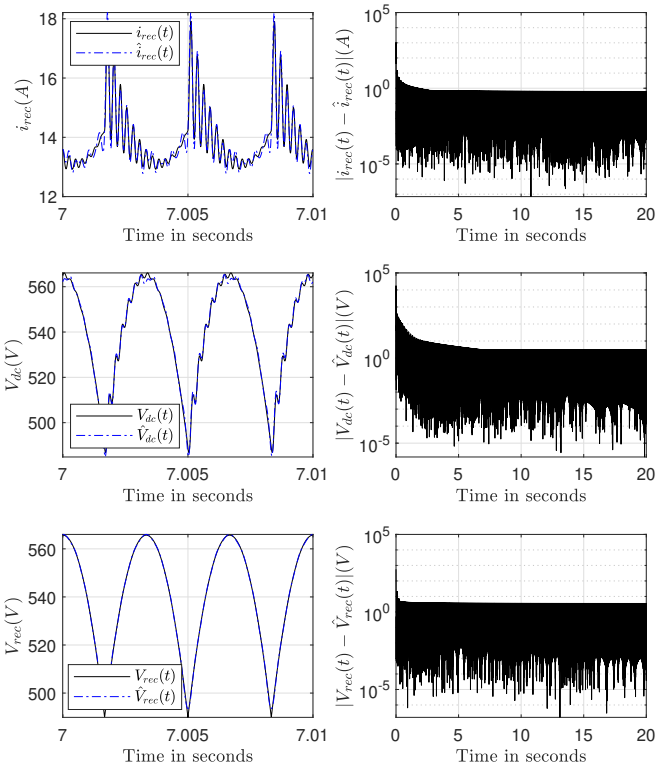

Fig. 3. Estimation of the rectification current $\hat{i}_{rec}(t)$, the DC-Link voltage $\hat{V}_{dc}(t)$ and the rectification voltage $\hat{V}_{rec}(t) = F^{\top}(t)\hat{\theta}(t)$.

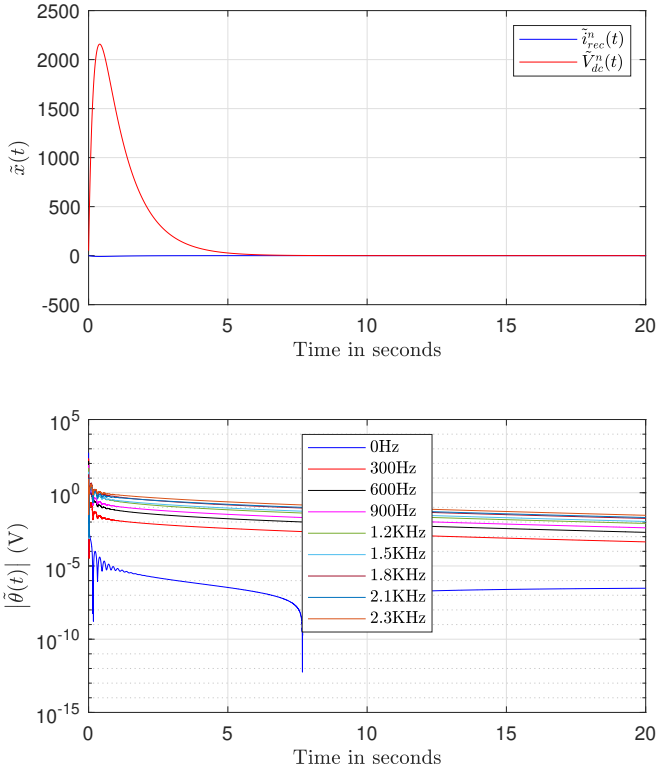

Fig. 4. Estimation of the harmonics of $V_{rec}(t)$.

VI. Conclusion

An adaptive observer for slim DC-Link AC drives is presented in the paper. In theory, as well as in numerical simulations, the designed observer is able to estimate the rectification current and the input voltage at the same time. The work is limited for slim DC-Link AC drives. Because of the reduced size of the DC-Link capacitor, we were able to estimate the amplitudes of the input voltage harmonics. The limitation is an intrinsic property of the system given that the only available measurement is $V_{dc}(t)$. Indeed, if the rectification current is measured, the input voltage can be always reconstructed even for large values of the DC-Link capacitance (see (5)).

References

[1] W. Roger and P. Haines, *HVAC systems design handbook*. McGraw-Hill, New York, 2010.

[2] J. Larminie and J. Lowry, *Electric vehicle technology explained*. John Wiley & Sons, 2012.

[3] C. G. Reuther, "Ehpnet: Water environment federation," 2000.

[4] N. Korolev, A. Kozyaruk, and V. Morenov, "Efficiency increase of energy systems in oil and gas industry by evaluation of electric drive lifecycle," *Energies*, vol. 14, no. 19, p. 6074, 2021.

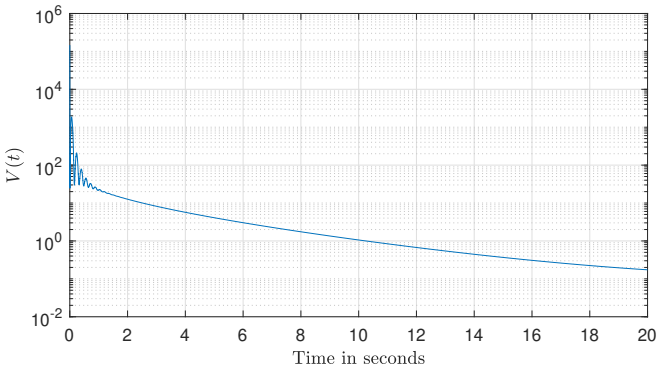

Fig. 5. The variation of the Lyapunov function $V(t)$ as a function of time.

[5] B.-G. Gu and K. Nam, "A dc-link capacitor minimization method through direct capacitor current control," *IEEE Transactions on Industry Applications*, vol. 42, no. 2, pp. 573–581, 2006.

[6] H. R. Andersen, R. Tan, and C. Kun, "3-phase ac-drives with passive front-ends with focus on the slim dc-link topology," in *2008 IEEE Power Electronics Specialists Conference*. IEEE, 2008, pp. 3248–3254.

[7] X. Chen and M. Kazerani, "Space vector modulation control of an ac–dc–ac converter with a front-end diode rectifier and reduced dc-link capacitor," *IEEE Transactions on power electronics*, vol. 21, no. 5, pp. 1470–1478, 2006.

[8] M. Hinkkanen, L. Harnefors, and J. Luorni, "Control of induction motor drives equipped with small dc-link capacitance," in *2007 European Conference on Power Electronics and Applications*. IEEE, 2007, pp. 1–10.

[9] R. Maheshwari, S. Munk-Nielsen, and K. Lu, "An active damping technique for small dc-link capacitor based drive system," *IEEE Transactions on Industrial Informatics*, vol. 9, no. 2, pp. 848–858, 2012.

[10] L. Mathe, L. Török, D. Wang, and D. Sera, "Resonance reduction for ac drives with small capacitance in the dc link," *IEEE Transactions on Industry Applications*, vol. 53, no. 4, pp. 3814–3820, 2017.

[11] W.-J. Lee and S.-K. Sul, "Dc-link voltage stabilization for reduced dc-link capacitor inverter," *IEEE Transactions on industry applications*, vol. 50, no. 1, pp. 404–414, 2013.

[12] J. E. Machado, R. Ortega, A. Astolfi, J. Arocas-Pérez, A. Pyrkin, A. A. Bobtsov, and R. Griñó, "An adaptive observer-based controller design for active damping of a dc network with a constant power load," *IEEE Transactions on Control Systems Technology*, vol. 29, no. 6, pp. 2312–2324, 2020.

[13] M. A. Hassan and Y. He, "Constant power load stabilization in dc microgrid systems using passivity-based control with nonlinear disturbance observer," *IEEE Access*, vol. 8, pp. 92 393–92 406, 2020.

[14] G. Kreisselmeier, "Adaptive observers with exponential rate of convergence," *IEEE Transactions on Automatic Control*, vol. 22, no. 1, pp. 2–8, 1977.

[15] P. Ioannou and J. Sun, "Robust adaptive control, Vol. 1, PTR Prentice-Hall Upper Saddle River," 1996.

[16] G. Luders and K. Narendra, "A new canonical form for an adaptive observer," *IEEE Transactions on Automatic Control*, vol. 19, no. 2, pp. 117–119, 1974.